

# THE LAPCAT-MR2 HYPERSONIC CRUISER CONCEPT

**J. Steelant and T. Langener\***

**\* ESA-ESTEC, Keplerlaan 1, 2201 AZ Noordwijk, Netherlands**

**Vehicle Design, Hypersonic Flight, Combined Cycle Engine, Dual-Mode Ramjet**

## Abstract

This paper describes the MR2, a Mach 8 cruise passenger vehicle, conceptually designed for antipodal flight from Brussels to Sydney in less than 4 hours. This is one of the different concepts studied within the LAPCAT II project [1]. It is an evolution of a previous vehicle, the MR1 based upon a dorsal mounted engine, as a result of multiple optimization iterations [2] leading to the MR2.4 concepts. The main driver was the optimal integration of a high performance propulsion unit within an aerodynamically efficient wave rider design, whilst guaranteeing sufficient volume for tankage, payload and other subsystems.

## Introduction

The aerodynamics for the MR2 is a waverider form based upon an adapted osculating cone method enabling to construct the vehicle from the leading edge while reducing integration problems between the aerodynamics and the intake.

The intake was constructed using streamtracing methods from an axisymmetric inward turning compression surface and was integrated on top of the waverider in a dorsal layout. The shape of the streamtraced intake surface changed during various evolutions of the vehicle but the final shape was elliptical with a ratio of semi-major to –minor axes of 3. This 3D shaped intake feeds a dual mode ramjet/scramjet combustion chamber and is foreseen to operate between M4.5 and M8. Below M4.5 an accelerator engine is required. Behind retracting door panels, a 2D-intake with moveable ramps is installed based upon the XB-70 intake and was shown numerically to provide the necessary mass flow and pressure recovery for the ATR engine downstream [3].

The nozzle was constructed in two sections; the first isentropic 2D nozzle has an area ratio of 3,

thus bringing the elliptical combustor cross section to a circular cross-section. During Ramjet-mode, this nozzle was used as a combustor that thermally choked, allowing for supersonic expansion in the second nozzle. The second nozzle itself was streamtraced from an axisymmetric isentropic expansion and truncated to a suitable length. Both nozzles were designed for cruise conditions.

The final vehicle is shown below in Figure 1 while specific details of the design are expanded upon in the next section.



**Figure 1 MR2 Vehicle**

## Discussion of sub-systems

### *WAVERIDER AND DORSAL ENGINE LAYOUT*

The deployment of a high-speed cruiser only makes sense for long haul flights with ranges up to antipodal destinations. Simply based on the Breguet range equation, at least a high L/D is necessary in combination with a low specific fuel consumption. Therefore, a waverider design was laid out to enable a  $L/D > 6$  for a cruise Mach number around 8. To maximize the available planform for lift generation and to optimize the internal volume, the engine was positioned on top. As the top surface of the wings

and the fuselage are nearly aligned with the flight vector, the lift is mainly generated by the windward side of the vehicle. This layout allowed furthermore to expand the jet to a large exit nozzle area (lower specific fuel consumption) without the need to perturb the external shape which would lead to extra pressure drag.

#### INWARD TURNING INTAKE

Though a conical shape for an air intake has intrinsically a minimal wetted area for a given compression ratio, one has still the choice between an inward versus outward turning intake. To evaluate the impact on the overall performance of the engine and its integration into the fuselage, a general analysis was carried out to address the pros and cons of both intake types. Values related to outward turning air intakes will be denoted with the subscript *out* whereas inward turning intakes by *inw*.

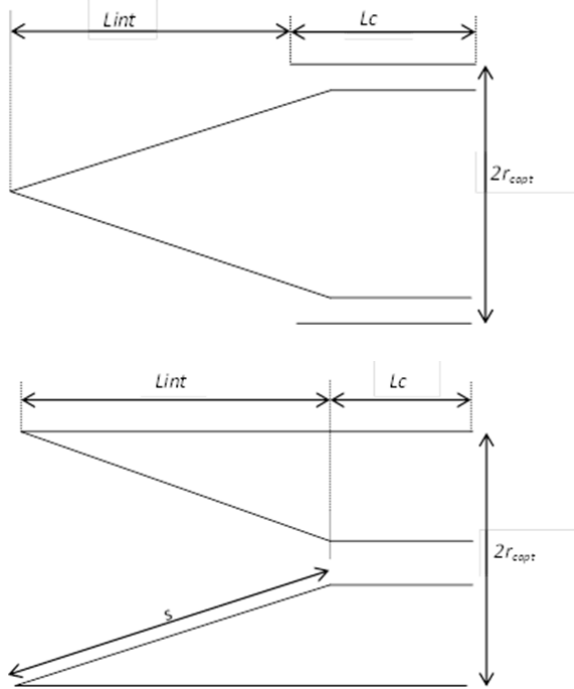


**Fig. 1: Outward (top) and Inward (bottom) turning conical air intakes.**

Based on the above figures, we start off with an identical air capture  $A_{capt}$ , conical intake length  $L_{int}$ , combustor + cowl length  $L_c$  and a compression ratio  $CR$  resulting in a combustor cross section  $A_{comb}$  defined as:

$$A_{comb} = \frac{A_{capt}}{CR} = \pi \frac{r_{capt}^2}{CR}$$

The radius of the combustor for the inward turning intake can be defined as function of  $A_{capt}$  and  $CR$ :

$$\begin{aligned} A_{comb,inw} &= \pi r_{c,inw}^2 \Rightarrow r_{c,inw} = \sqrt{\frac{A_{comb}}{\pi}} \\ &= \sqrt{\frac{A_{capt}}{\pi CR}} = \frac{r_{capt}}{\sqrt{CR}} \end{aligned}$$

The corresponding wetted combustor + cowl area  $S_{wet,c,int}$  is then given as:

$$S_{wet,c,inw} = 2\pi r_{c,inw} L_c = 2\pi \frac{r_{capt} L_c}{\sqrt{CR}}$$

For the outward turning intake, the height of the combustor can be defined as follows:

$$\begin{aligned} A_{comb,out} &\cong 2\pi r_{capt} h_{c,out} \Rightarrow h_{c,out} = \frac{A_{comb}}{2\pi r_{capt}} \\ &= \frac{A_{capt}}{2\pi CR} \sqrt{\frac{\pi}{A_{capt}}} = \frac{1}{2CR} \sqrt{\frac{A_{capt}}{\pi}} \\ &= \frac{r_{capt}}{2CR} \end{aligned}$$

The corresponding wetted combustor + cowl area is then given as (the factor 2 applies for the double amount of inner walls compared to an internally turning intake):

$$S_{wet,c,out} = 2 \times 2\pi r_{capt} L_c$$

The ratio of the wetted combustor areas can hence be written as:

$$\frac{S_{wet,c,out}}{S_{wet,c,inw}} = 2\sqrt{CR}$$

For a contraction ratio e.g.  $CR = 9$ , the wetted combustor area is 6 times higher for an externally versus an internally turning intake. However, for an internal compression, there is also an extra wetted area stemming from the casing which is not present for an external compression. Assuming a worst case scenario where we have a completely axi-symmetric casing (from an operational point of view this is not desirable due to not-startability addressed later on), the wetted intake casing areas are respectively:

$$S_{wet,case,inw} = 2\pi r_{capt} (L_{int} + L_c)$$

$$S_{wet,case,out} = 2\pi r_{capt} L_c$$

The wetted area on the conical intake, whether internal or external, is given as:

$$S_{wet,cone} = \pi r_{capt} s \approx \pi r_{capt} \sqrt{L_{int}^2 + r_{capt}^2}$$

For a specific flight dynamic pressure  $q_\infty$  and a given skin friction  $C_f$ , one can calculate the viscous casing drag:

$$\begin{aligned} D_{out,case} &= C_f q_\infty S_{wet,case,out} = C_f q_\infty 2\pi r_{capt} L_c \quad (1) \\ D_{inw,case} &= C_f q_\infty S_{wet,case,inw} \\ &= C_f q_\infty 2\pi r_{capt} (L_{int} + L_c) \end{aligned}$$

For the drag estimation on the intake cone, cowls and inside the combustion chambers, one can apply the general approach that the velocity is nearly constant throughout the internal flowpath at these high flight speeds. This means that the dynamic pressure at the cowl and in the combustion chamber can be linked to the flight dynamic pressure as:

$$\begin{aligned} q_c &= \frac{1}{2} \rho_c v_c^2 = \frac{1}{2} \frac{\dot{m}}{A_{comb}} v_c \approx \frac{1}{2} \frac{\rho_\infty v_\infty A_{capt}}{A_{comb}} v_\infty \\ &= q_\infty \frac{A_{capt}}{A_{comb}} = q_\infty CR \end{aligned}$$

Hence for the above given value of  $CR=9$ , the dynamic pressure in the combustor is 9 times larger than the flight dynamic pressure. The drag generated within the ducts consisting of the cowls and combustors is given respectively as:

$$\begin{aligned} D_{c,inw} &= C_f q_{comb} S_{wet,c,inw} = C_f q_\infty S_{wet,c,inw} CR \\ &= C_f q_\infty 2\pi \sqrt{CR} r_{capt} L_c \\ D_{c,out} &= C_f q_{comb} S_{wet,c,out} \\ &= C_f q_\infty S_{wet,c,inw} CR 2\sqrt{CR} \\ &= C_f q_\infty 4\pi CR r_{capt} L_c \quad (2) \end{aligned}$$

Assuming an identical skin friction coefficient, the ratio of both drag components is hence identical to the ratio of wetted areas:

$$\frac{D_{c,out}}{D_{c,inw}} = 2\sqrt{CR}$$

The drag on the cone surface itself is approximated as:

$$D_{cone} = C_f q_\infty S_{wet,cone} \quad (3)$$

The total drag for the external compression intake can then be expressed as the contribution form (1), (2) and (3):

$$\begin{aligned} D_{tot,out} &= C_f q_\infty \pi r_{capt} s + C_f q_\infty 4\pi CR r_{capt} L_c \\ &\quad + C_f q_\infty 2\pi r_{capt} L_c \\ D_{tot,out} &= C_f q_\infty \pi r_{capt} (s + 2CR L_c + L_c) \end{aligned}$$

$$D_{tot,inw} = C_f q_\infty \pi r_{capt} (s + \sqrt{CR} L_c + L_c + L_{int}) \quad (1)$$

Hence the difference in drag between both intakes is at most:

$$D_{tot,out} - D_{tot,inw} = C_f q_\infty \pi r_{capt} ((2CR - \sqrt{CR})L_c - L_{int}) \quad (2)$$

One has to consider that the casing for the internally turning intake doesn't necessarily needs to be taken as a drag force on the intake. Depending on the layout, if this casing can be integrated cleverly into the fuselage it can actually serve as part of the lifting geometry of the vehicle. In case of the LAPCAT MR2, near half of this casing is located on the windward side generating lift, which otherwise needed to be provided by extra wing surface. Moreover, in order to assure a startable intake, the particular choice of the positioning of the elliptical streamtracing shape slightly below the axis of the conical template flowfield resulted in a nearly triangular opening at the top. This opening doesn't contribute nor to the external drag or the intake cone. Hence, the last term  $L_{int}$  in the above equations (1) and (2) can be dropped at best along with a reduction of  $s$  representing the effective exposed surface for a non-closed internal turning surface. In any case, for the considered vehicles,  $L_{int}$  is about 3 to 4 times larger than  $L_c$ . With a  $CR = 9$ , the multiplication factor in the above equation ranges between 11 to 12. As a ratio we have:

$$\frac{D_{tot,out}}{D_{tot,inw}} = \frac{s + 2CRL_c + L_c}{s + \sqrt{CR}L_c + L_c + L_{int}}$$

After some simplifications ( $s \approx L_{int}$ ), one can reduce the ratio to:

$$\frac{D_{tot,out}}{D_{tot,inw}} \approx \frac{L_{int} + 2CRL_c + L_c}{L_{int} + \sqrt{CR}L_c + L_c + L_{int}}$$

For the same values for  $L_{int}$ ,  $L_c$  and  $CR$  as used previously, the above ratio results into a factor ranging from 2 up to 3 (the latter number due to a reduced conical surface for a stream-traced intake). The evolution of the drag ratio is shown in Figure 2. This total drag increase with 200% to 300% is mainly linked to the 6 times larger drag within the annular combustor compared to the circular duct.

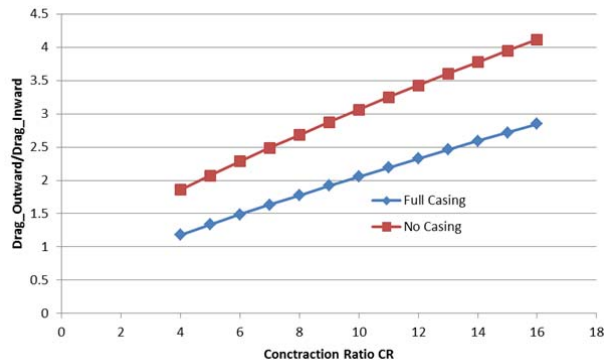


**Figure 2: Drag ratio for outward vs inward turning intakes; colours representing fully and not-optimized integration into a hypersonic cruiser.**

*INTAKE/AERODYNAMICS INTEGRATION*

The front view of the MR2 in Figure 3 shows how the intake is integrated within the waverider shaped fuselage. The elliptical capture shape (12m x 4m) used for the streamtracing procedure was projected to the most forward plane which served as the leading edge of the waverider.

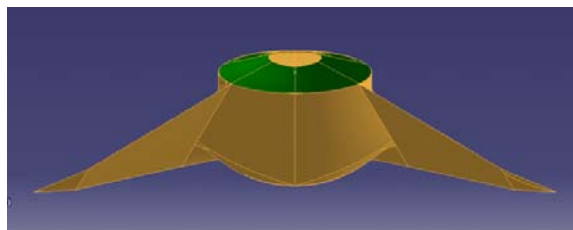


**Figure 3: Front view of MR2 showing the integrated intake and waverider leading edge.**

Figure 4 shows a zoom of the integrated region. The waveriders elliptical leading edge does not extend from 0° up to -180° but instead goes from about -28° to -152°. The portion missing between -152° and -180° is circled in the figure.

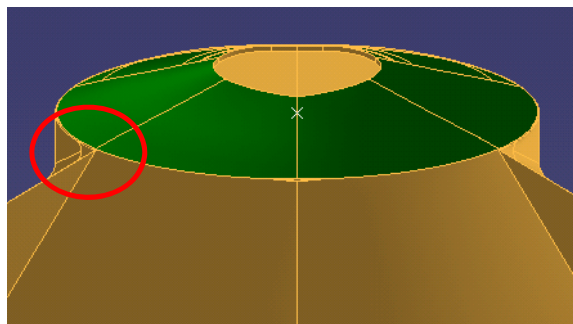


**Figure 4: Zoom of intake/waverider integrated region.**

Although this introduced a small drag surface downstream of the leading edge when the oblique angle between the two was blended out, it was necessary to limit the wingspan of the waverider. Due to the boundary layer displacement correction that has been applied to the intake geometry, the cross-section of the combustor is not exactly elliptical.

*DUAL-MODE RAMJET PROPULSION MODEL*

The Dual Mode Ramjet unit was modelled from 0D/1D engineering tools up to 3D CFD codes with detailed combustion chemistry at different levels of details [4] [5]. This allowed a general layout of the combustor and a detailed injector strut layout ensuring a good mixing and combustion efficiency.

This detailed CFD analysis further allowed to assess the spillage drag and their effect on the overall installed thrust.

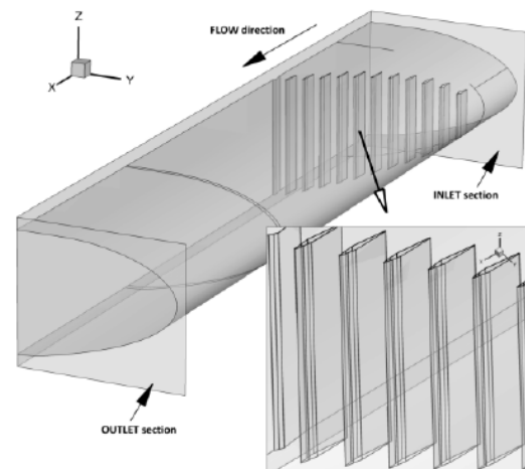


**Figure 5: Layout of Injector strategy.**

*ATR ENGINE INTEGRATION*

The Air-Turbo-Rocket (ATR), [6] [7], [8] inlet in the MR2 design were integrated as shown in Figure 6. A detailed CFD study was conducted to optimize the different ramp settings. A mass capture of over 50% could be achieved between Mach 1.2 and 4.5 matching the required mass capture for the ATR engine based upon an expander cycle. Also the needed pressure recovery could be achieved.

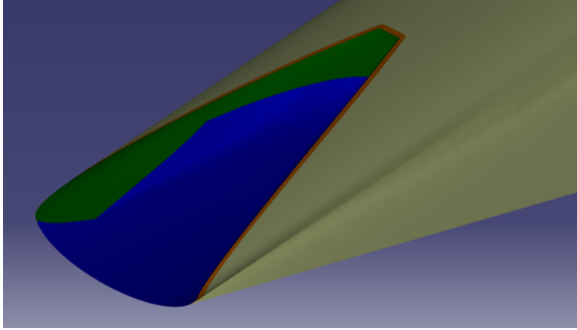
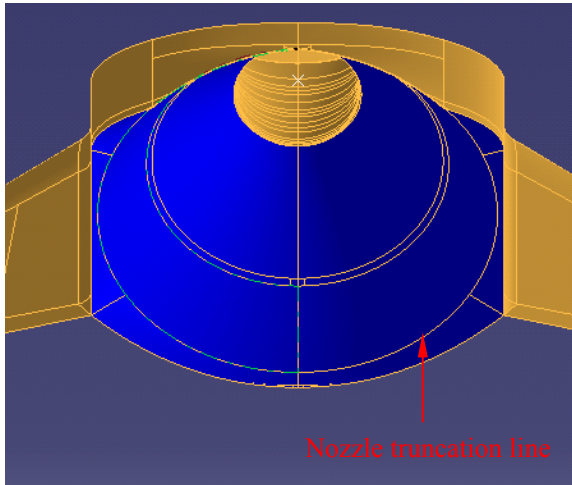


**Figure 6: LAPCAT-MR2 ATR air intake diversion door opening side view**

*NOZZLE DESIGN AND INTEGRATION*

The nozzle contour was designed using the method of characteristics (MOC) and afterwards streamtraced using a similar method as for the intake. The complete nozzle consisted of an initial 2D isentropic expansion followed by a 3D isentropic expansion. Whilst this is not the most efficient way of expanding the flow, it provided a discontinuity in the surface to fix the thermally induced normal shock during Ram-mode.

The 2D expansion was designed for an area ratio of three so that the combustor ellipse was brought to a circle. This then minimized the length of the following 3D nozzle. Despite this, the 3D nozzle was 75m long and so was truncated to 43m to fit with the vehicle length. This would seem to produce quite a drop in thrust but in reality the final 30% of an isentropic expansion produces relatively little thrust when the low pressures and skin friction are considered.



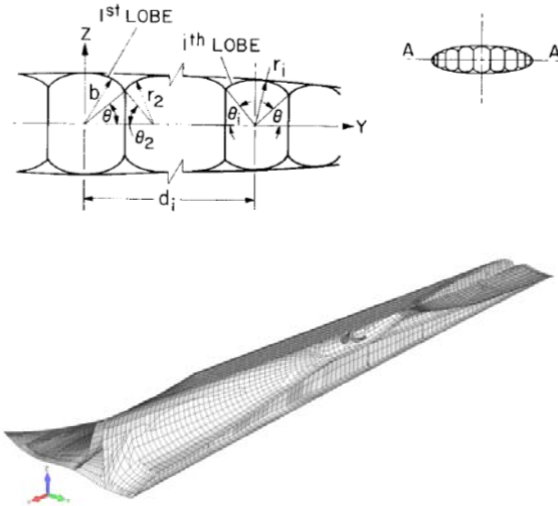
**Figure 7: Zoom of MR2 nozzle. The blue region denotes a thrust surface.**

Figure 7 shows a zoom of the nozzle with the truncation line. In order to properly integrate the nozzle into the vehicle a rough taper was inserted around the nozzle which in effect increased its area ratio. CFD computations showed that the overall thrust of the nozzle was approximately the same as calculated for the un-truncated nozzle using the isentropic expansion and the 0.85 nozzle efficiency.

*STRUCTURE*

The waverider shape was designed with structural integrity in mind but a rigorous structural mass analysis is needed to properly assess the vehicle performance. The waverider shape does not conform to typical vehicle topologies and so methods such as WAATS method produced very different results depending on the interpretation of different parameters. A deviation of up to 40-50% was found between different estimates of the structural weight.

However, specific studies have focused on the structural masses of waveriders indicating that the lower estimate of structural mass found using WAATS has some validity [9]. A lobed design technique where the fuel tanks are incorporated into the vehicle load structure (Figure 8) were proposed.



**Figure 8: Multi-lobe internal structure and corresponding FEM model.**

A finite element analysis was conducted of the multi-lobed structure which confirmed its feasibility with other studies in literature and the lower mass estimates of the WAATS analysis. No uncertainty factor for this rather new and innovative structural design method is included whereas a 71% increase

of the ideal body and wing weights to account for cut-outs, gage penalties, fasteners, and machining constraints is included.

*HYDROGEN FUEL*

In LAPCAT-I [10], it was clearly shown that liquid hydrogen is the only fuel able to achieve antipodal flight due to its high specific energy content. Hydrocarbons lead too fast to a large GTOW prohibiting a fuel-efficient acceleration to cruise speed. Liquid hydrogen was selected as the fuel for the vehicle due to its very high specific energy content. Despite its low density and the inherently low volume on board of a waverider concept, the available internal tankage volume allowed more than 180 tons of fuel mass taking into account thermal insulation and ullage volumes. The different tank compartments which were modelled in a detailed CAD design made it possible to further calculate the shift of the CoG of the fuel at different fill levels.

*MASS BREAKDOWN*

The mass estimations for the other subsystems were based upon existing correlations derived from supersonic and hypersonic vehicles (based upon the WAATS weight analysis tool) or directly obtained by provided weights in the open literature (e.g. landing gear). The total Gross Take-Off Weight ended up to 400tons of which 60tons was allocated to the payload and about 180tons for the fuel. The mass breakdown for the other subsystems are detailed in Figure 9. The acronyms used in the legend are representing the different systems on-board and are listed here below:

- aerodynamic surfaces: wings and control surfaces: WSURF
- body structure: WBODY
- Thermal Protection System (TPS): WTPS
- propulsion: engines and tanks: WPROPU
- take-off and landing gear: WGEAR
- power supply: WPOWER
- payload: WPAYLOAD (i.e. passengers, crew, cabin, luggage,...)
- fuel: WFUEL
- margin: WMARGIN

The related weight values are embedded into the figure.

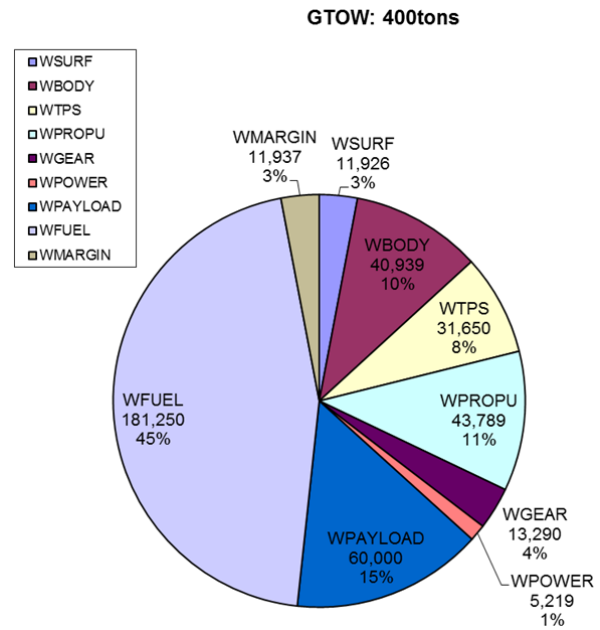


**Figure 9: GTOW Mass Breakdown of LAPCAT MR2.4**

*TRAJECTORY*

The trajectory calculations were performed using ASTOS [11], a three/six degrees of freedom trajectory code in a cartesian coordinate system with its origin at the centre of a spherically rotating planet.

The aerodynamic and propulsive forces are based upon engineering methods or detailed nose-to-tail computations. This entails also complete thermodynamic cycles for the ATR and DMR.

The range trajectory included a 400 km subsonic cruise to reach the ocean from take-off at most European airports prior to acceleration to supersonic. This acceleration phase of the trajectory could take up to 45% of the fuel mass. It was shown in [6] that the mission Brussels – Sydney as a representation of an antipodal flight is in principally feasible, given the available vehicle layout and the databases for the engines and for the aerodynamic performance. The flight time to Sydney would be around 2h55m whereas all the available fuel on board would be consumed. The missions to Tokyo need 2h13m and the flight to Los Angeles 2h20m. All three simulated routes lead over the North Pole and cross the Bering Strait in order to avoid supersonic cruise over inhabited land.



**Fig. 2 View on complete trajectory with pole crossing and Bering Strait passage.**

#### TRIMMING

Once the full trajectory was known along with the vehicle weight change and the CoG-shift, a trimming analysis could be carried out. However, a particular difficulty is related to the influence of the engine flowpath on the overall pitching moment. Additionally to the external aerodynamics, one needs to take into account the effect of intake spillage along the full Mach range together with the different moments induced both by engine on and off operation. Thanks to a detailed Nose-to-Tail computation, both for engine on and off conditions at different Mach numbers allowed to evaluate the trimmability of the vehicle. It indicated that both the presence of canards and ailerons are needed.

#### Conclusions

In the presented paper the basic principle and design choices of the LAPCAT MR2 hypersonic cruiser concept have been described with particular attention to the choice of the intake and its integration into the aircraft layout as a dorsal mounted engine. By this way a combined high aerodynamic and propulsion efficiency could be guaranteed which is a prerequisite to assure a long range without excessive fuel burns and gross take-off weights.

Also the other major subsystems have been concisely addressed allowing to perform a first feasibility study and a global performance. The analysis indicated that a hypersonic cruiser at Mach

8 for antipodal flight is conceptually feasible provided liquid hydrogen is used as a fuel. With a GTOW of 400tons and a fuel burn of 180tons, the antipodal range from Brussels to Sydney is achievable within 3 hours.

Presently, further elaborations are ongoing with respect to the optimization of an integrated advanced thermal protection system including on-board power generation while exploiting the large heat capacity of the on-board cryogenic fuel.

#### Acknowledgements

This work was performed within the ‘Long-Term Advanced Propulsion Concepts and Technologies II’ project investigating high-speed transport. LAPCAT II, coordinated by ESA-ESTEC, is supported by the EU within the 7th Framework Programme Theme7 Transport, Contract no.: ACP7-GA-2008-211485. Further info on LAPCAT II can be found on [http://www.esa.int/techresources/lapcat\\_II](http://www.esa.int/techresources/lapcat_II).

#### Bibliography

- [1] J. Steelant, "Sustained Hypersonic Flight in Europe: Technology Drivers for LAPCATII," in *16th AIAA/DLR/DGLR International Space Planes and Hypersonic System Technologies Conference*, Bremen, Germany, 2009.
- [2] N. Murray, J. Steelant and A. Mack, "Conceptual Design of a Mach 8 Hypersonic Cruiser with Dorsal Engine," in *Sixth European Symposium on Aerothermodynamics for Space Vehicles*, Versailles, France, 2008.
- [3] C. Meerts and J. Steelant, "Air Intake Design for the Acceleration Propulsion Unit of the LAPCAT-MR2 Hypersonic Aircraft," in *5th European Conference for Aeronautics and Space Sciences (EUCASS)*, Munich, 2013.
- [4] T. Langener, J. Steelant, P. Roncioni, P. Natale and M. Marini, "Preliminary Performance Analysis of the LAPCAT-MR2 by means of Nose-to-Tail Computations," in *18th AIAA/3AF International Space Planes and Hypersonic Systems and Technologies Conference*, Tours, France, 2012.

- [5] P. Roncioni, P. Natale, M. Marini, T. Langener and J. Steelant, "Numerical Simulations of the LAPCAT MR-2 Vehicle Scramjet Engine," in *ISABE-2013-1656*, Busan, S. Korea, 2013.
- [6] T. Langener, S. Erb and J. Steelant, "Trajectory Simulation and Optimization of the LAPCAT MR2 Hypersonic Cruiser Concept," in *ICAS 2014*, St. Petersburg, Russia, 2014.
- [7] V. Fernández-Villace, G. Paniagua and J. Steelant, "Installed performance evaluation of an air turbo-rocket expander engine," *Aerospace Science and Technology*, vol. 35, pp. pp. 63-79, 2014.
- [8] I. Rodríguez Miranda, V. Fernández Villacé and G. Paniagua, "Modeling, Analysis, and Optimization of the," *Journal of Propulsion and Power*, p. DOI: 10.2514/1.B34781, 2013.
- [9] A. Bardenhagen, H. Kossira and W. Heinze, "Weight Estimation of Hypersonic Waveriders within the Integrated Design Program Prado-Hy," in *AIAA 96-4546*,, 1996.
- [10] J. Steelant, "Achievements obtained for sustained hypersonic flight within the LAPCAT project," in *15th AIAA International Space Planes and Hypersonic Systems and Technologies Conference*, Dayton, OH, 2008.
- [11] ASTOS Solutions GmbH, *ASTOS 7 - ASTOS Model Library*, Unterkirnach, Germany, 2011.

### Copyright Statement

The authors confirm that they, and/or their company or organization, hold copyright on all of the original material included in this paper. The authors also confirm that they have obtained permission, from the copyright holder of any third party material included in this paper, to publish it as part of their paper. The authors confirm that they give permission, or have obtained permission from the copyright holder of this paper, for the publication and distribution of this paper as part of the ICAS 2014 proceedings or as individual off-prints from the proceedings.